Journal of Luminescence 180 (2016) 158–162

Contents lists available at ScienceDirect

Journal of Luminescence

journal homepage: www.elsevier.com/locate/jlumin

Full Length Article

Site distortion in Li_2SrSiO_4: Influence on Pr^{3+} emission and application in wLED

Liangliang Zhang, Jiahua Zhang*, Xia Zhang, Zhendong Hao, Guo-Hui Pan, Huajun Wu

[a] State Key Laboratory of Luminescence and Applications, Changchun Institute of Optics, Fine Mechanics and Physics, Chinese Academy of Sciences, 3888 Eastern South Lake Road, Changchun 130033, China

ARTICLE INFO

Article history:
Received 20 April 2016
Received in revised form
10 August 2016
Accepted 16 August 2016
Available online 24 August 2016

Keywords:
Phosphor
WLED
Luminescence
Site distortion
Li_2SrSiO_4

ABSTRACT

Luminescence of Pr^{3+} in Li_2SrSiO_4 showed a broader f–f emission band compared with YAG:Pr^{3+}. Atom parameters of Li_2SrSiO_4 crystal were refined to provide data for quantifying the distortion of [SrO8] polyhedron. The distortion of [SrO8] was compared with that of [YO8] polyhedron in YAG to show the different Pr^{3+} environments in Li_2SrSiO_4 and YAG. Then, Pr^{3+} was co-doped with Eu^{2+} in Li_2SrSiO_4 to provide a single phosphor for wLEDs. Energy transfer processes from 5d of Eu^{2+} to both $^3P_2$ and $^1D_2$ of Pr^{3+} were observed. The interaction type between Eu^{2+}–Pr^{3+} was proved to be dipole-quadrupole and kinetics of the energy transfer process was discussed based on Inokuti–Hirayama model.

1. Introduction

In the past decades, white light-emitting diodes (wLEDs) have seen remarkable breakthroughs in efficiency by using a blue InGaN chip to pump YAG:Ce^{3+} yellow phosphor. However, the color-rendering index (CRI) of such a wLED (<80) is too low to be applied for illumination [1,2]. This is ascribed to the deficiency of red component in the spectrum. Thus many efforts have been paid to find new yellow phosphors with improved red component in recent years [3–5]. Li_2SrSiO_4:Eu^{2+} phosphor [6] is one of the most studied yellow phosphors with better CIE values and high thermal stability superior to YAG:Ce^{3+}. Li_2SrSiO_4:Eu^{2+} shows a strong orange–yellow emission band with maximum at 562 nm. The phosphor can be excited by 400-470 nm blue light and is practical to blue LED chip. The wLED fabricated with Li_2SrSiO_4:Eu^{2+} shows improved red component compared to YAG:Ce^{3+} with similar efficiency. Thus Li_2SrSiO_4:Eu^{2+} is believed to be a candidate yellow phosphor for blue LED chip.

In recent years, many efforts have been paid to improve color rendering property and efficiency of Li_2SrSiO_4:Eu^{2+} phosphor. Ce^{3+} was co-doped in Li_2SrSiO_4:Eu^{2+} to enhance emission intensity of Eu^{2+} [7]. Energy transfer progress from Ce^{3+} to Eu^{2+} was observed [8]. The interaction type between Ce^{3+}–Eu^{2+} was proved to be dipole–dipole and the critical energy transfer distance was calculated to be 27.62 Å [9]. However, Kim et. al. [10] proved that the energy transfer progress contributes little to the enhanced luminescence. They suggested that the increased emission intensity is mainly from stabilized Li^+ vacancies, inhibited oxidization of Eu^{2+} by Ce^{3+} substitution. Song et. al. [11] modified Li_2SrSiO_4:Eu^{2+} phosphor with Si_3N_4 and increased the intensity with 1.9 times. Temperature property was also improved with only 10% decrease of intensity at 150 °C. Ca^{2+}, Ba^{2+} and Mg^{2+} were introduced into Li_2SrSiO_4 to substitute for Sr^{2+} by Li et. al [12]. As results, the emission was red-shifted from 562 nm to 594 nm which promised a warmer white light output. Dy^{3+}, Sm^{3+}, Eu^{3+} were introduced into Li_2SrSiO_4 with emission at 573 nm, 594 nm and 590 nm respectively by Erdogmus [13]. Dy^{3+}, Eu^{3+} co-doped Li_2SrSiO_4 was reported to realize white output by Zhang et. al [14]. Li_2SrSiO_4 phosphor was also studied for other applications. For example, Ce^{3+}, Er^{3+} co-doped Li_2SrSiO_4 was reported by Li et. al. [15] to convert 360 nm light into 1530 nm for Ge solar cells. Ce^{3+}, Pr^{3+} co-doped Li_2SrSiO_4 was reported by Chen et. al. [16] for plant growth LED. Eu^{2+}, Dy^{3+} co-doped Li_2SrSiO_4 was reported by Cheng et. al. [17] as a long-lasting phosphor.

Pr^{3+} ion is a well-known red center with sharp emission lines at ~610 nm. For example, Pr^{3+} is co-doped into YAG:Ce^{3+} to increase a red emission line at 608 nm with CRI of 83 [18]. Thus Pr^{3+} is expected to increase red component in Li_2SrSiO_4:Eu^{2+} phosphor. Emission of Pr^{3+} is originated from $4f^m$ levels. According to Judd–Ofelt theory, the emission intensity between two $4f^m$ levels is determined by the odd parity terms of the crystal field,

* Corresponding author.
E-mail address: zhangjh@ciomp.ac.cn (J. Zhang).

http://dx.doi.org/10.1016/j.jlumin.2016.08.033
0022-2313/

which can be affected by site distortion [19,20]. Li_2SrSiO_4 crystallizes in hexagonal symmetry with space group of $P3_121$. Eu^{2+} occupies Sr^{2+} site in Li_2SrSiO_4 which is coordinated with eight oxygen atoms. Sr^{2+} site is believed to have a high level of distortion for its low Stokes shift [21]. However, there are still difficulties to quantify the site distortion.

In this paper, two definitions, eccentric distance and sphericity is introduced to quantify the site distortion of Sr^{2+} site in Li_2SrSiO_4. Instead of considering bond length and bond angular, we only considered the coordinate atoms. A new method to calculate the geometric center (centroid) of the coordinate atoms was developed by Zunic et. al. [22]. Eccentric distance is the distance that center atom shifting from the centroid. This definition is a measurement of crystal field distortion caused by off-center effect of center atom in an idea sphere crystal field. Sphericity estimates the degree that the coordination polyhedron deviating from a sphere. Sphericity shows the crystal field distortion caused by non-spherical-shape distribution of the coordinate atoms around their centroid. Thus, eccentric distance and sphericity are useful to determine the distortion of crystal field.

We reported Pr^{3+} doped and Eu^{2+}, Pr^{3+} co-doped Li_2SrSiO_4 phosphor. Li_2SrSiO_4:Pr^{3+} phosphor shows a broader emission bands than YAG:Pr^{3+}. The broad red emission property shows potential application in wLEDs. Thus, Pr^{3+} ion is co-doped with Eu^{2+} to enhance the red component. The energy transfer process between Eu–Pr is also discussed.

2. Experiential

The samples were synthesized by solid-state reaction. Appropriate amounts of Li_2CO_3, $SrCO_3$, and SiO_2 were weighted as starting materials according to nominal composition. The raw materials were fully grounded in an agate mortar and pressed into a graphite crucible. Mixtures of raw materials were firstly preheated at 600 °C for 6 h at atmosphere environment. Then, raw materials were grounded and sintered at 850 °C for 6 h in reductive atmosphere.

The photoluminescence (PL) and photoluminescence excitation (PLE) spectra were measured by HITACHI F-4500 spectrometer equipped with a 150 W xenon lamp. Both the excitation and emission slits were set at 2.5 nm. X-ray diffraction (XRD) patterns were collected in a Bruker powder diffractometer. The XRD data were collected in range of 5-80° with step size of 0.02° and count time of 5 s/step. The decay curves were measured by FL920 fluorimeter (Edinburgh Instruments). The excitation wavelength is 450 nm with a pulse time of 1 ns.

3. Results and discussion

Rietveld refinement is carried out to investigate the crystal structure with undoped Li_2SrSiO_4. Since Li_2SrSiO_4 is isotopic with Li_2EuSiO_4, the atomic coordinates of Li_2EuSiO_4 is employed as the starting model for Rietveld refinement. However, cell parameters of Li_2SrSiO_4 are quite different from that of Li_2EuSiO_4 and, thus, resulting in failure of the refinement. To get proper cell parameters for refinement, indexing of the powder pattern is performed by Dicvol06, a powder patterns indexing program with dichotomy method. Two lattice system is indexed by Dicvol06: orthorhombic lattice with Figure of Merit M(20)=260.6, F(20)=264.7 and hexagonal lattice with M(20)=300.7, F(20)=328.2, as shown in Table 1. Both results are reliable since their Figures of Merit are much larger than the threshold value 15. Other indexing programs by different indexing methods are introduced to confirm the results. Indexing by McMaille, a powder patterns indexing software by Monte Carlo and grid search method, shows that hexagonal lattice is the optimal solution, as shown in Table 1. Indexing by TREOR90, a powder indexing program by Heuristic Search method, also shows that hexagonal is the best lattice systems for Li_2SrSiO_4. Spacegroup determination is performed subsequently by Chekcell program based on the indexing result. However, ten spacegroup is determined: $P6_2$, $P6_4$, $P6_222$, $P6_422$, $P3_1$, $P3_2$, $P3_112$, $P3_121$, $P3_212$, and $P3_221$. It is impossible to separate these groups based on powder diffraction data alone. Luckily, Li_2SrSiO_4 is isotopic with Li_2EuSiO_4 which is approved to be $P3_121$ space group by single crystal diffraction data [23]. The refined cell parameter is a=b=5.0261 Å, c=12.4635 Å, α=β=90°, γ=120°. These cell parameters are employed as the starting model for Rietveld refinement and R-factors, R_p and R_{wp}, are converged to 5.23% and 7.16% respectively, as shown in Fig. 1a. Electron-density map of Li_2SrSiO_4 is calculated by using the reverse Fourier transform of structure factor. As shown in Fig. 1b(a=0), and Fig. 1d (c=0). The calculated density map shows perfect agreement with the refined structure.

Fig. 2 is the XRD patterns of Li_2SrSiO_4:xPr^{3+} and Li_2SrSiO_4:-0.01Eu^{2+}, yPr^{3+} samples. No impure phase or change of the crystal type is observed by Pr^{3+} and/or Eu^{2+} doping. The emission and excitation spectra of Li_2SrSiO_4:Pr^{3+} are shown in Fig. 3a. The excitation spectrum monitoring 609 nm emission is consisted of three peaks ascribed to the transition between $^3H_4 \rightarrow {}^3P_0$, $^3P_1$, $^3P_2$, respectively. The excitation peaks at 443 nm and 451 nm makes Li_2SrSiO_4:Pr^{3+} suitable for blue LED chips. The emission peak of Li_2SrSiO_4:Pr^{3+} consists of a main peak at 609 nm and four shoulder peaks at 605 nm, 598 nm, 592 nm, and 584 nm, respectively. The five peaks are overlapped with each other, which makes Li_2SrSiO_4:Pr^{3+} displaying a broad red emission peak. As shown in Fig. 3a, the bandwidth of Li_2SrSiO_4:Pr^{3+} is broader than YAG:Pr^{3+}.

Luminescence of Pr^{3+} is mainly affected by the coordination environment. Sr^{2+} site in Li_2SrSiO_4 is coordinated with 8 oxygen atoms (marks as [SrO8] union). Y^{3+} site in YAG is also coordinated with 8 oxygen atoms (marks as [YO8] union). However, Pr^{3+} in Li_2SrSiO_4 shows emission between $^3P_0 \rightarrow {}^3H_6$, $^1D_2 \rightarrow {}^3H_4$, $^3P_0 \rightarrow {}^3F_2$, $^3I_1 \rightarrow {}^3H_6$, and $^3P_1 \rightarrow {}^3H_6$, while Pr^{3+} in YAG only shows emission between $^1D_2 \rightarrow {}^3H_4$. According to Judd–Ofelt theory, the emission intensity between two $4f^n$ levels is determined by the odd parity terms of the crystal field. The odd parity can be increased with distorted coordination. Thus, we compare the level of distortion between [SrO8] and [YO8], as shown in Fig. 3b. It is obvious that [SrO8] shows great divergence compared with [YO8]. Based on the

Table 1
Indexing results of different powder pattern indexing program.

Program	Bravaisb lattice	a/Å	b/Å	c/Å	α/°	β/°	γ/°	V/Å^3	Figure of merit		
									M (20)	F (20)	Rp
Dicvol06	P hexagonal	5.0234	5.0234	12.4564	90	90	120	272.21	300.7	328.2	–
	P orthorhombic	4.350	2.512	12.456	90	90	90	136.08	264.7	165.3	–
McMaille	P hexagonal	5.0230	5.0230	12.4557	90	90	120	272.156	313.93	338.81	0.022
TREOR 90	P hexagonal	5.0225	5.0225	12.454	90	90	120	272.070	216	229	–

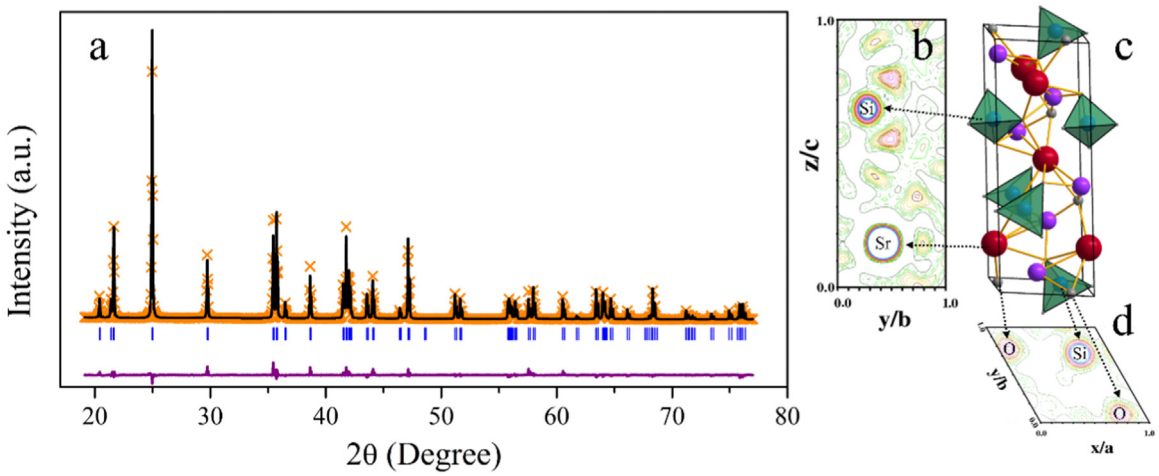

Fig. 1. Rietveld refinement plot of un-doped SrAlSi4N7 (a). Observed (cross), calculated (black line), and difference profile (bottom line) of the XRD pattern are plotted in the same range. Bragg peak positions are shown as vertical bars. Crystal structure (c) and electron-density map (b), (d) of Li_2SrSiO_4 based on the refined structure.

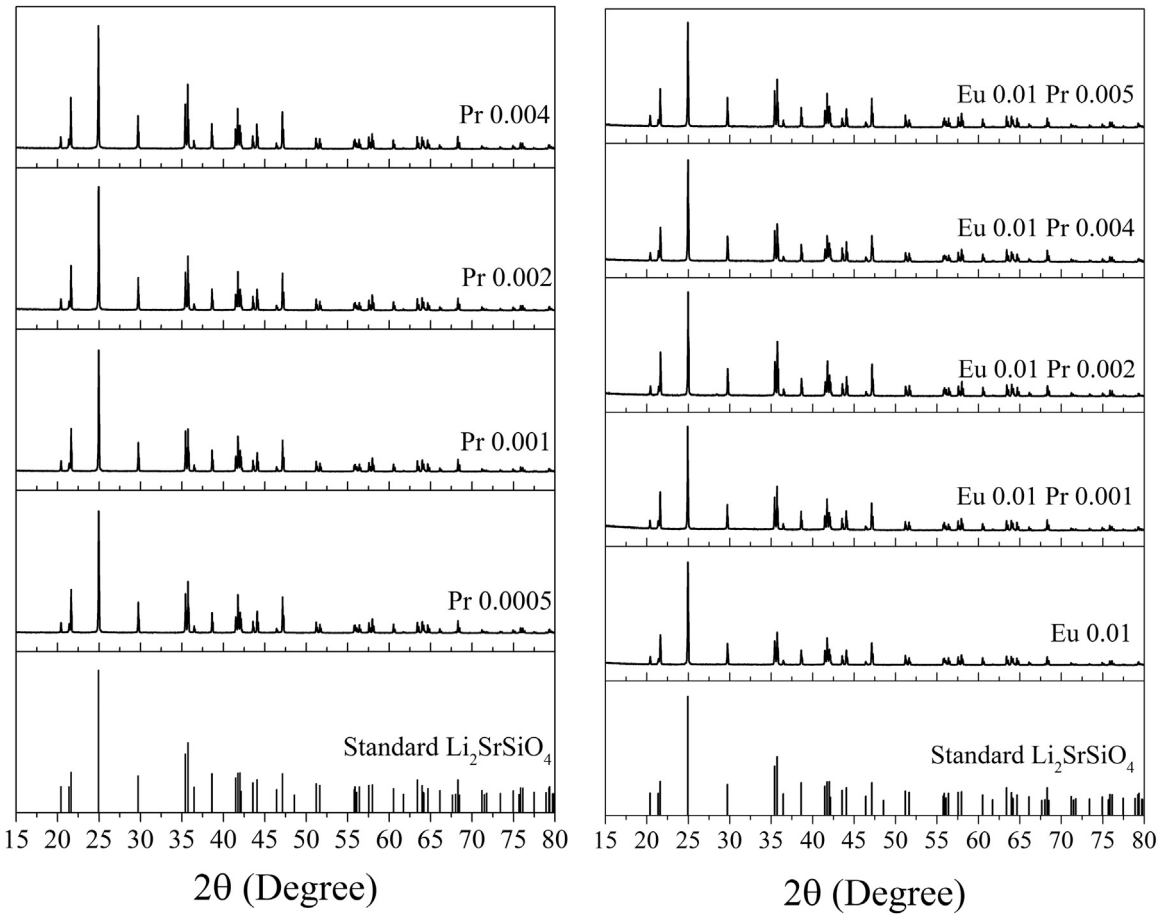

Fig. 2. XRD patterns of Li_2SrSiO_4:xPr^{3+} and Li_2SrSiO_4:0.01Eu^{2+}, yPr^{3+}.

result of Rietveld refinement, it can be calculated that the centroid (geometric center) of 8 oxygen atoms of [SrO8] is located at (0.0088, 0.3998, 0.1834). The coordinate of Sr atom is (0, 0.4202, 0.1667). Thus, Sr atom shows a 0.25 Å shift (eccentric distance) from the centroid of coordination polyhedron. In [YO8], Y atom locates at the centroid of the 8 coordination oxygen atoms. This indicates that Pr^{3+} in Li_2SrSiO_4 suffering from a unique distorted crystal field originated from the off-center effect. To determine the distribution regularity of the coordination O atoms, the sphericity of coordination polyhedron around Sr is calculated to be 0.941. In [YO8], the sphericity is 0.985. This indicates that Pr^{3+} in Li_2SrSiO_4 also suffers a much more distorted crystal field originated from irregular distribution of ligands. The distortions will increase the odd parity terms of crystal field and, therefore, increase the intensity of transition between different $4f^n$ states of Pr^{3+}.

The average Pr–O distance in Li_2SrSiO_4, according to the Rietveld refinement result, is 2.63 Å, much larger than that of YAG (2.43 Å). The longer Pr–O distance accounts for the blue shift of

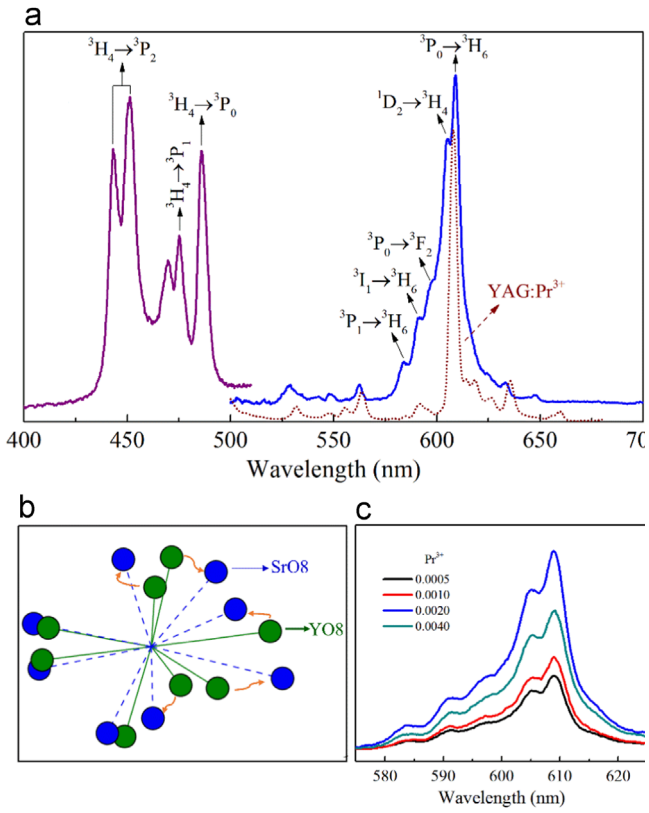

Fig. 3. (a) Emission (450 nm) and excitation (609 nm) spectra of $Li_2SrSiO_4:Pr^{3+}$. The dotted line is the emission spectrum of YAG:Pr^{3+} excited by 450 nm. (b) Schematic [SrO8] and [YO8] by putting both Sr atom and Y atom at original point. (c) Emission spectra of $Li_2Sr_{1-x}SiO_4:xPr^{3+}$ excited by 450 nm.

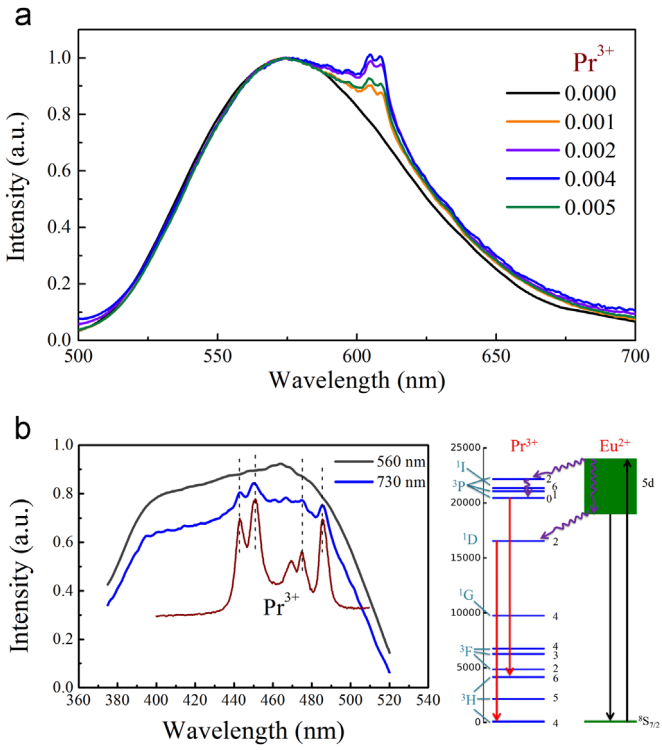

Fig. 4. Emission spectra of $Li_2SrSiO_4:0.01Eu^{2+},yPr^{3+}$ excited by 450 nm (a).Excitation spectra (b) of $Li_2SrSiO_4:Pr^{3+}$ (brown line, 730 nm), $Li_2SrSiO_4:Eu^{2+},Pr^{3+}$ (blue line, 730 nm where emission of Eu^{2+} is undetectable), $Li_2SrSiO_4:Eu^{2+}$ (black line, 560 nm). Energy level sketch map for Pr^{3+} and Eu^{2+} (c). (For interpretation of the references to color in this figure legend, the reader is referred to the web version of this article.)

$^1D_2\rightarrow{}^3H_4$ emission in $Li_2SrSiO_4:Pr^{3+}$ (605 nm) compared with YAG:Pr^{3+} (~608 nm). Emission spectra of $Li_2Sr_{1-x}SiO_4:xPr^{3+}$ with various x is shown in Fig. 3c. The shape of the emission are not changed with different x. The strongest emission is achieved when $x=0.002$. This indicates that concentration quenching effect is appeared.

The broader emission of Pr^{3+} in Li_2SrSiO_4 makes it suitable for application in wLEDs where red component is deficient. Thus, Pr^{3+} is co-doped with Eu^{2+} to offer a new phosphor. Fig. 4a is the emission spectra of $Li_2Sr_{0.986}SiO_4:0.01Eu^{2+}$, yPr^{3+} excited by 450 nm. An increased red emission is observed and broadens the highest peak of Eu^{2+} into a range from 560 nm to 610 nm. The co-doped Pr^{3+} increases the red component of $Li_2SrSiO_4:Eu^{2+}$ phosphor and will further increase the color rendering property of the wLED. Fig. 4b is the excitation spectra of $Li_2Sr_{0.986}SiO_4:0.01Eu^{2+}$, $0.004Pr^{3+}$ monitoring 560 nm (Eu^{2+} emission) and 730 nm ($^3P_0\rightarrow{}^3F_4$ transition of Pr^{3+}) respectively. When monitoring 730 nm emission of Pr^{3+}, a broad absorption band of Eu^{2+} is observed. This phenomenon indicates the energy transfer process from Eu^{2+} to Pr^{3+}.

The interesting question is that 605 nm ($^1D_2\rightarrow{}^3H_4$) emission of Pr^{3+} is stronger than 609 nm ($^3P_0\rightarrow{}^3H_6$) in Eu^{2+}, Pr^{3+} co-doped samples (Fig. 4a) while 605 nm emission is weaker in Pr^{3+} single-doped samples (Fig. 3a). This can be ascribed to the energy transfer process form Eu^{2+} to Pr^{3+}. As shown in Fig. 4b, Eu^{2+} shows absorption at 400 nm, much shorter than the absorption of $^3H_4\rightarrow{}^3P_2$ of Pr^{3+}. This indicates that upper edge of 5d level of Eu^{2+} is higher than $^3P_2$ level of Pr^{3+}. Thus an energy transfer routine from 5d of Eu^{2+} to $^3P_2$ of Pr^{3+} is reasonable. This process will increase both $^3P_0\rightarrow{}^3H_6$ (609 nm) and $^1D_2\rightarrow{}^3H_4$ (605 nm) transition. Eu^{2+} also show absorption at ~500 nm, longer than the absorption of $^3H_4\rightarrow{}^3P_0$ of Pr^{3+}. This indicates that lower 5d edge of Eu^{2+} is below $^3P_0$ level of Pr^{3+}. Thus an energy transfer routine from 5d of Eu^{2+} to $^1D_2$ of Pr^{3+} is expected. This process will increase the emission of $^1D_2\rightarrow{}^3H_4$ (605 nm) alone. Thus 605 nm emission becomes stronger in Eu^{2+}, Pr^{3+} co-doped samples. The energy level sketch map for Pr^{3+} and Eu^{2+} is shown in Fig. 4c.

As shown in Fig. 4a, intensity of the Pr^{3+} emission reaches maximum when $y=0.004$. This is different from the previous result in $Li_2Sr_{1-x}SiO_4:xPr^{3+}$ samples where the strongest emission is achieved at $x=0.002$ (Fig. 3c). This indicates that the energy transfer process shows advantage over concentration quenching effect when $0.002\le y\le 0.004$.

Fig. 5a is the decay curves of $Li_2Sr_{0.99-y}SiO_4:0.01Eu^{2+},yPr^{3+}$ by monitoring 560 nm emission. The decay curves change from exponential to non-exponential with increasing Pr^{3+} concentration, demonstrating the energy transfer from Eu^{2+} to Pr^{3+}. The energy transfer process can be expressed by Inokuti–Hirayama formula:

Where I_d represents decay curve of the donor and I_0 represents decay curve of donor in the absence of accepter. α is a rate constant for energy transfer. s is a coefficient with value of 6, 8, and 10 respectively for dipole-dipole, dipole-quadrupole, and quadrupole–quadrupole interaction. n_A is the number of acceptor ions per unit volume. It can be derived that $\log\{-\ln[I_d/I_0]\}$ shows a linear dependence on $\log(t)$ with slope of $3/s$. As shown in Fig. 5b, s is calculated to be 7.96 which is approximate to 8. Thus the electric interaction type of Eu–Pr is dipole–quadrupole. Such an interaction type is lesser effective compared with that of Ce–Pr in YAG which is dipole–dipole interaction. It can also be approved that $\ln[I_d/I_0]$ shows liner relationship against $t^{3/m}$ with slope of $-[4\pi\Gamma(1-3/s)n_A\alpha^{3/s}]/3$. We have plotted $\mathrm{Ln}(I_d/I_0)$ vs $t^{3/8}$ for $Li_2Sr_{0.986}SiO_4:0.01Eu^{2+}$, $0.004Pr^{3+}$, as shown in Fig. 5c. The best fitting to the decay curve yields a transfer constant $\alpha=2.454\times10^{-54}\ \mathrm{cm}^8\ \mathrm{s}^{-1}$. Critical energy transfer distance

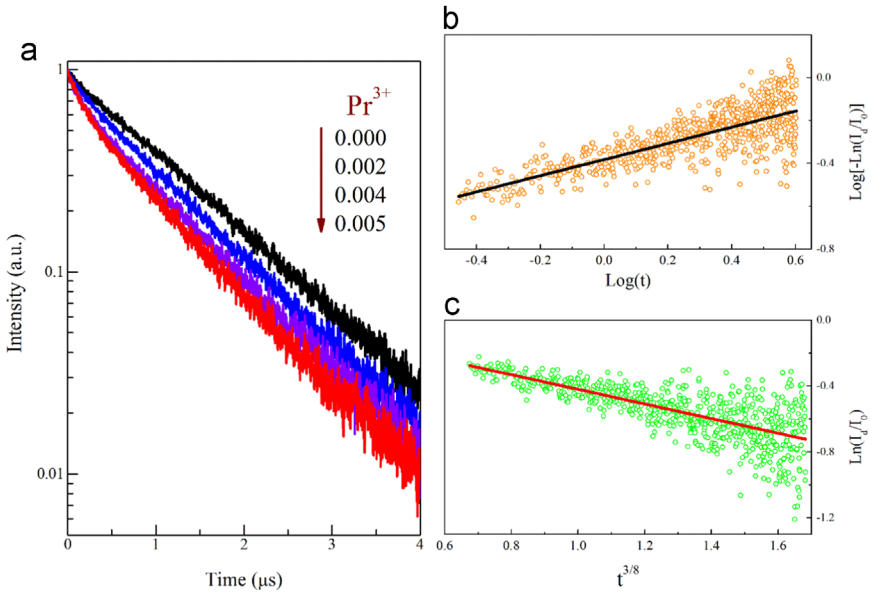

Fig. 5. Decay curves of Li_2SrSiO_4:0.01Eu^{2+}, yPr^{3+} monitoring 560 nm (a). Relationship between Log[− Ln(I(t)/I_0(t))] and Log(t) (b), and plot of ln(I_d/I_0) vs $t^{3/8}$ (c) of Li_2SrSiO_4:0.01Eu^{2+},0.004Pr^{3+}.

R_0 is the distance between an isolated donor–accepter pair that the energy transfer rate is the same with the spontaneous radiation of donor. R_0 can be calculated to be 3.6 Å based on the relation $R_0^s = \alpha \times \tau_0$. τ_0 is the lifetime of donor without accepters around. τ_0 is 1.06 μs and is obtained by integrating the decay curve of $Li_2Sr_{0.99}SiO_4$:0.01Eu^{2+}. R_0 for Eu–Pr transfer is smaller than that of Ce–Pr (8.1 Å) transfer in YAG.

4. Conclusions

The crystal structure of Li_2SrSiO_4 is confirmed by Rietveld refinement. The refined cell and atom parameters are used to determine the site distortion afterwards. Results show that [SrO8] polyhedron in Li_2SrSiO_4 suffers an off-center of Sr and a larger distorted non-spherical-shape distribution of O compared with [YO8] in YAG. In Eu^{2+}, Pr^{3+} co-doped Li_2SrSiO_4, the red component is increased. Energy transfer process from Eu^{2+} to Pr^{3+} is observed and the electric interaction type of Eu–Pr is confirmed to be dipole–quadrupole. Critical energy transfer distance R_0 of Eu–Pr transfer is 3.6 Å, much smaller than that of Ce–Pr transfer in YAG.

Acknowledgments

This work was partially supported by the National Natural Science Foundation of China (Grant no. 61275055, 11274007 and 51402284) and the Natural Science Foundation of Jilin province (Grant no. 20140101169JC, 20150520022JH and 20160520171JH).

References

[1] P. Dai, C. Li, X. Zhang, J. Xu, X. Chen, X. Wang, Y. Jia, X. Wang, Y. Liu, Light Sci. Appl. 5 (2016) e16024.
[2] Y. Liu, J. Zhang, C. Zhang, J. Xu, G. Liu, J. Jiang, H. Jiang, Adv. Opt. Mater. 3 (2015) 1096.
[3] L. Zhang, J. Zhang, X. Zhang, Z. Hao, H. Zhao, Y. Luo, ACS Appl. Mater. Interfaces 5 (2013) 12839.
[4] W. Lü, W. Lv, Q. Zhao, M. Jiao, B. Shao, H. You, J. Mater. Chem. C 3 (2015) 2334.
[5] X. Li, J. Budai, F. Liu, J. Howe, J. Zhang, X. Wang, Z. Gu, C. Sun, R. Meltzer, Z. Pan, Light Sci. Appl. 2 (2013) e50.
[6] M. pardha Saradhi, U.V. Varadaraju, Chem. Mater. 18 (2006) 5267.
[7] X. Zhang, H. He, Z. Li, T. Yu, Z. Zou, J. Lumin. 128 (2008) 1876.
[8] Z. Wei, Y. Wang, X. Zhu, J. Guan, W. Mao, J. Song, Chem. Phy. Lett. 648 (2016) 8.
[9] H. He, R. Fu, Y. Cao, X. Song, Z. Pan, X. Zhao, Q. Xiao, R. Li, Opt. Mater. 32 (2010) 632.
[10] T. Kim, H. Lee, C. Lin, T. Kim, R. Liu, T. Chan, S. Im, Appl. Phy. Lett. 96 (2010) 061904.
[11] K. Song, F. Zhang, D. Chen, S. Wu, P. Zheng, Q. Huang, J. Jiang, J. Xu, H. Qin, Mater. Res. Bull. 70 (2015) 309.
[12] Y. Li, Z. Ci, Y. Peng, Y. Wang, C. Liu, Mater. Res. Bull. 61 (2015) 146.
[13] E. Erdogmus, J. Appl. Spec. 6 (2014) 956.
[14] Z. Zhang, X. Shen, Y. Peng, Y. Ren, Z. Mao, Lumin. 30 (2015) 72.
[15] Y. Li, C. Ni, C. Lin, F. Pan, R. Liu, J. Wang, Opt. Mater. 36 (2014) 1871.
[16] J. Chen, C. Guo, Z. Yang, T. Li, J. Zhao, J. Am. Ceram. Soc. (2015) 1.
[17] S. Cheng, X. Xu, J. Han, J. Qiu, B. Zhang, Powder Technol. 276 (2015) 129.
[18] L. Wang, X. Zhang, Z. Hao, Y. Luo, J. Zhang, X. Wang, J. Appl. Mater. 108 (2010) 093515.
[19] A. Sengupta, S.V. Godbole, P.K. Mohapatra, M. Iqbal, J. Huskens, W. Verboom, J. Lumin. 148 (2014) 174.
[20] O. Ravi, C.M. Reddy, B.S. Reddy, B.D.P. Raju, Opt. Commun. 312 (2014) 263.
[21] S. Levshow, I. Berezovskaya, N. Efryushina, B. Zadneprovskii, V. Dotsenko, Inorg. Mater. 47 (2011) 285.
[22] T.B. Zunic, E. Makovicky, Acta Crystallogr 52 (1996) 78.
[23] B. Haferkorn, G. Meyer, Z. Anorg. Allg. Chem. 624 (1998) 1079.